

Linear and Weakly Nonlinear Models of Wind Generated Surface Waves in Finite Depth

A. Latifi^{1†}, M. A. Manna², P. Montalvo² and M. Ruivo²

¹ *Department of Physics, Faculty of Sciences, Qom University of Technology, Qom, Iran,*
² *Université Montpellier, Laboratoire Charles Coulomb UMR 5221, F-34095, Montpellier, France.*

†Corresponding Author Email: latifi@qut.ac.ir

(Received January 14, 2017; accepted August 8, 2017)

ABSTRACT

This work regards the extension of the Miles' and Jeffreys' theories of growth of wind-waves in water of finite depth. It is divided in two major sections. The first one corresponds to the surface water waves in a linear regime and the second one to the surface water waver considered in a weak nonlinear, dispersive and anti-dissipative regime. In the linear regime, we extend the Miles' theory of wind wave amplification to finite depth. The dispersion relation provides a wave growth rate depending to depth. A dimensionless water depth parameter depending to depth and a characteristic wind speed, induces a family of curves representing the wave growth as a function of the wave phase velocity and the wind speed. We obtain a good agreement between our theoretical results and the data from the Australian Shallow Water Experiment as well as the data from the Lake George experiment. In a weakly nonlinear regime the evolution of wind waves in finite depth is reduced to an anti-dissipative Kortewegde Vries-Burgers equation and its solitary wave solution is exhibited. Anti-dissipation phenomenon accelerates the solitary wave and increases its amplitude which leads to its blow-up and breaking. Blow-up is a nonlinear, dispersive and anti-dissipative phenomenon which occurs in finite time. A consequence of anti-dissipation is that any solitary waves' adjacent planes of constants phases acquire different velocities and accelerations and ends to breaking which occurs in finite space and in a finite time prior to the blow-up. It worth remarking that the theoretical amplitude growth breaking time are both testable in the usual experimental facilities. At the end, in the context of wind forced waves in finite depth, the nonlinear Schrödinger equation is derived and for weak wind inputs, the Akhmediev, Peregrine and Kuznetsov-Ma breather solutions are obtained.

Keywords: Surface waves; Wind waves; Interface waves; Rogue waves; Blow-up; Asymptotic models; Miles's mechanism; Jeffreys' mechanism.

1. INTRODUCTION

Surface water waves and their generation by wind is a fascinating problem. The starting point is the Navier-Stoke equation for air and water. This is a very interesting problem both from the physical and the mathematical point of view. Theoretically, it is impossible to find an exact solution to this equation, but it is possible to obtain particular solutions by using various approximations and assumptions.

On of the mechanism wave growth is the action of wind. The *action balance equation* represents the dynamics of these processes. In deep water it reads (Janssen (2004))

$$\frac{\partial}{\partial t} \mathcal{N} + \vec{\nabla} \cdot (\vec{c}_g \mathcal{N}) = S \quad (1)$$

where $\mathcal{N} = E/\omega$ is the *action density* with ω the wave

frequency and \vec{c}_g the group velocity observed in the moving frame of the wave and the source

$$S = S_{in} + S_{nl} + S_{ds} + \dots \quad (2)$$

S_{in}, S_{nl}, S_{ds} respectively representing the effects of the wind input, non-linear interactions and dissipation due to white capping.

The pioneering surface wind-waves growth theories start with Jeffreys (1925; 1926), Phillips (1957) and Miles (1997) and continue with modern works of Janssen (1991) and Belcher & Hunt (1993). The focal point of these works is the computation of the term S_{in} in (2). Later, in order to calculate S_{in}, S_{nl}, S_{ds} (Janssen, 2004) some numerical approaches were developed.

Nonetheless, these theories are not adequate to

correctly describe wind generated near-shore waves, since they are limited to the *deep water domain*.

In *finite depth* the source S contain more terms

$$S = S_{in} + S_{nl} + S_{ds} + S_{bf} + S_{tri} + \dots \quad (3)$$

In this case, S_{in} is strongly influenced by the finite depth h and must be recalculated. S_{bf} and S_{tri} represent bottom friction and triad nonlinear wave interactions.

At our knowledge, the only theoretical extensions of these theories to finite depth were recently done by Montalvo *et al.* (2013a); (Montalvo, Dorignac, Manna, Kharif, and Branger) and Montalvo *et al.* (2013b) (Montalvo, Kraenkel, Manna, and Kharif). The aim of those works was to provide a surface wind-waves growth theory in finite depth with the Euler equations as outset. The purpose was twofold, in one hand to provide mathematical laws able to qualitatively reproduce some features of the fields experiments on growth rate evolution of finite depth wind-waves, and in the other hand to supply a theoretical basis allowing to go beyond the empirical laws. To carry on this task, authors have introduced an extension of the well known Miles' theory (Miles, 1997) to the finite depth and an adequate parametrization to the Jeffreys' theory (Jeffreys, 1925; Jeffreys; 1926). In Montalvo *et al.* (2013b) (Montalvo, Kraenkel, Manna, and Kharif) was studied the wind action on the evolution of a wave-packet and in (Manna *et al.* (2014) (Manna, Montalvo, and Kraenkel) was studied the evolution in time of a normal Fourier mode k under the coupled action of weakly nonlinearity, dispersion and anti-dissipation.

This work is based on these last development and is devoted to give *l'etat de l'art* in the field. The paper is divided in five sections, Section 2. and Section 4. concern respectively the linear and the nonlinear approaches. In section 3. we show that the theoretical linear laws we derived in Section 2. are able to reproduce the known experimental facts. Finally section 5. draws the conclusions.

2. WIND GENERATED SURFACE WAVES. THE LINEAR REGIME

Let a fix rectangular Cartesian frame with origin O and axes (x,y,z) , where O_z is the upward vertical direction and let us localize the fluid particles in this frame. We will only consider a sheet of fluid parallel to the xz plane since we assume a translational symmetry along y . The plane of the interface at rest is characterized by $z = 0$ and $z = \eta(x,t)$ characterizes the perturbed airwater interface. Consequently, $\eta(x,t) < z < +\infty$ is the region occupied by the air, and the water is located between the bottom at $z = -h$ and the interface $z = \eta(x,t)$. The water as well as the air are assumed to be inviscid and incompressible. The unperturbed air flow is a prescribed mean shear flow. We disregard the air turbulence and assume its dynamic to be linear, building a *quasi-laminar theory*.

2.1 The Linearized Water Dynamics

In the water domain we consider the Euler equations for finite depth. $u(x,z,t)$ is the horizontal and $w(x,z,t)$ is the vertical velocity of the fluid. The linearized equations of motion and in the water domain read (Lighthill, 1925)

$$\rho_w \frac{\partial u}{\partial t} = -\frac{\partial P}{\partial x}, \rho_w \frac{\partial w}{\partial t} = -\frac{\partial P}{\partial z}, \quad (4)$$

with the reduced pressure $P(x,z,t)$ defined as follows

$$P(x,z,t) = P(x,z,t) + \rho_w gz - P_0, \quad (5)$$

where $P(x,z,t)$ is the pressure, g the gravitational acceleration, ρ_w is the water density and P_0 , the atmospheric pressure. The continuity equation reads

$$\frac{\partial u}{\partial x} + \frac{\partial w}{\partial z} = 0 \quad (6)$$

and the boundary conditions at $z = -h$ and at $z = \eta(x,t)$ are $w(-h) = 0, \partial_t \eta = w(0)$. The continuity of the pressure across the air/water interface

$$P(x,\eta,t) = P_a(x,\eta,t) + \rho_w g \eta - P_0. \quad (7)$$

where P_a is the air pressure evaluated at $z = \eta$. It worth remarking that this is a vital assumption for the growth mechanism.

The linear equations system (4)-(7) can be solved, assuming normal mode solutions as

$$\begin{aligned} P &= \mathcal{P}(z) \exp(ik(x-ct)), \\ u &= \mathcal{U}(z) \exp(ik(x-ct)), \\ w &= \mathcal{W}(z) \exp(ik(x-ct)), \\ \eta &= \eta_0 \exp(ik(x-ct)), \end{aligned} \quad (8)$$

where k is the wavenumber, c the phase speed and η_0 is a constant. Using equations (4), (6), (7) and (8) we obtain

$$w(x,z,t) = \frac{-ikc \sinh k(z+h)}{\sinh kh} \eta_0 \exp(ik(x-ct)), \quad (9)$$

$$u(x,z,t) = \frac{kc \cosh k(z+h)}{\sinh kh} \eta_0 \exp(ik(x-ct)), \quad (10)$$

$$P(x,z,t) = \frac{k \rho_w c^2 \cosh k(z+h)}{\sinh kh} \eta_0 \exp(ik(x-ct)), \quad (11)$$

The phase speed c is unknown in equations (8). To determine c we have to consider the continuity equation (7), and boundary conditions which yields

$$\begin{aligned} \rho_w \eta_0 \exp(ik(x-ct)) \{c^2 k \coth kh - g\} \\ + P_0 = P_a(x,\eta,t). \end{aligned} \quad (12)$$

Notice that in the problem without interface (single

domain) $P_a(x, \eta, t) = P_0$ and (12) gives the usual expression $c^2 = c_0^2 = (g/k) \tanh(kh)$. But of course in the present paper, the determination of c needs the use of the air pressure evaluated at $z = \eta$.

2.2 The Linearized Air Dynamics

Let us consider the linearized equations governing a steady air flow, with a prescribed mean horizontal velocity $U(z)$ depending only on the vertical coordinate z . We are going to study perturbations of $U(z)$. From this point, the subscript a stands for air. With $P_a(x, z, t) = P_a(x, z, t) + \rho_a g z - P_0$, we have the following equations

$$\frac{\partial u_a}{\partial x} + \frac{\partial w_a}{\partial z} = 0, \tag{13}$$

$$\rho_a \left\{ \frac{\partial u_a}{\partial t} + U(z) \frac{\partial u_a}{\partial x} + \frac{dU(z)}{dz} w_a \right\} = -\frac{\partial P_a}{\partial x}, \tag{14}$$

$$\rho_a \left\{ \frac{\partial w_a}{\partial t} + U(z) \frac{\partial w_a}{\partial z} \right\} = -\frac{\partial P_a}{\partial z}, \tag{15}$$

which have to be completed with the kinematic boundary condition for air, evaluated at the aerodynamic sea surface roughness z_0 located just above the interface. In this work, we consider z_0 will be a constant, independent from the sea state which is a widely used approximation, first proposed by (Charnock, 1955). We have to notice that for the datasets used in next sections, the wind speed ranges are such that the roughness may be seen as a constant (Fairall *et al.* 1996, Fairall, Grachev, Bedard, and Nishiyama). The kinematic boundary condition reads

$$\frac{\partial \eta}{\partial t} + U(z_0) \frac{\partial \eta}{\partial x} = w_a(z_0). \tag{16}$$

The common profile of $U(z)$ used to describe the vertical distribution of the horizontal mean wind speed is a logarithmic profile. This assumption is valid within the lowest portion of the airside of the marine boundary layer (Garratt *et al.* 1996; Garratt, Hess, Physick, and Bougeault). It can also be justified with scaling arguments and solution matching between the near-surface air layer and the geostrophic air layer (see Tennekes, 1972).

$$U(z) = U_1 \ln(z/z_0), U_1 = \frac{u_*}{k}, k \approx 0.41, \tag{17}$$

where u_* is the friction velocity and k the Von Kármán constant. So, Eq. (16) can be reduced to $\partial_t \eta = w_a(z_0)$. This equation describes the influence of the perturbation of the water surface on the vertical profile of wind speed. Then we consider normal mode solution as in (8) and we add the following boundary conditions on W_a and P_a ,

$$\lim_{z \rightarrow z_0} W_a = W_a, \tag{18}$$

$$\lim_{z \rightarrow +\infty} P_a = 0. \tag{19}$$

$$\lim_{z \rightarrow +\infty} \left(\frac{dW_a}{dz} + kW_a \right) = 0, \tag{20}$$

This means that the vertical component of the wind speed is enforced by the wave movement at the sea surface and the disturbance plus its derivative vanish at infinity. Now, using equations (13)-(15) and (19) yields to

$$w_a(x, z, t) = W_a \exp(ik(x - ct)), \tag{21}$$

$$u_a(x, z, t) = \frac{i}{k} \frac{\partial W_a}{\partial z} \exp(ik(x - ct)), \tag{22}$$

$$P_a(x, z, t) = ik \rho_a \exp(ik(x - ct)) \int_z^\infty [U - c] W_a d\zeta. \tag{23}$$

Removing the pressure from the Euler equations, we find the well-known Rayleigh equation (Rayleigh (1880)) $\forall z \setminus z_0 < z < +\infty$ (inviscid Orr-Sommerfeld equation)

$$(U - c) \left(\frac{d^2 W_a}{dz^2} - k^2 W_a \right) - \frac{d^2 U}{dz^2} W_a = 0. \tag{24}$$

This equation is singular at $z_c = z_0 e^{ck/u_*} > z_0 > 0$, where $U(z_c) = c$. We recall that this model disregards any kind of turbulence, and the critical height z_c is set above any turbulent eddies or other non-linear phenomena. In equations (21)-(24) neither $W_a(z)$ nor c are known. In order to find c , we have to calculate $P_a(x, \eta, t)$. We obtain

$$P_a(x, \eta, t) = P_0 - \rho_a g \eta + ik \rho_a \exp(ik(x - ct)) \int_{z_0}^\infty [U(z) - c] W_a(z) dz. \tag{25}$$

In the above equation, since we are studying the linear problem, the lower integration bound is taken at the constant roughness height z_0 instead of $z = \eta$. Using equation (18) to eliminate the term $ik \rho_a \exp(ik(x - ct))$ the equation (25) in (12) yields

$$g(1 - \varepsilon) + c \frac{\varepsilon k^2}{W_0} I_1 - c^2 \left\{ \frac{\varepsilon k^2}{W_0} I_2 + k \coth(kh) \right\} = 0, \tag{26}$$

where $\varepsilon = \rho_a / \rho_w$ is a small parameter ($\rho_a / \rho_w \sim 10^{-3}$) and the integrals I_1 and I_2 are defined as follow

$$I_1 = \int_{z_0}^\infty U W_a dz, \quad I_2 = \int_{z_0}^\infty W_a dz. \tag{27}$$

Equation (26) is the dispersion relation of the problem. If $h \rightarrow \infty$, we obtain the expression (3.7) of the reference (Beji and Nadaoka(2004)). the dispersion relation (26) may be approximated as

$$c = c_0 + \varepsilon c_1 + O(\varepsilon^2). \tag{28}$$

The explicit form of c_1 will be calculated in the next section. Therefore, we are going to be able to find $W_a(z)$ by solving (24) by putting $c = c_0$, which means that we consider the order zero in ε of c .

2.3 The Wave Growth rate

$W_a(z)$ is a complex function and therefore c is complex too. Its imaginary part $\Im(c)$ gives the growth rate of $\eta(x,t)$ defined by

$$\gamma = k \Im(c). \tag{29}$$

For theoretical and numerical results concerning the growth rate γ see (Young and Verhagen, 1996a) and (Young and Verhagen, 1996b). In these studies, two dimensionless parameters δ and θ_{dw} defined as follows

$$\delta = \frac{gh}{U_1^2}, \quad \theta_{dw} = \frac{1}{U_1} \sqrt{\frac{g}{k}}. \tag{30}$$

The dimensionless parameter δ , measures the influence of the finite fluid depth on the growth rate of $\eta(x,t)$. The parameter θ_{dw} can be seen as a *theoretical analogous of the deep water wave age*. It measures the relative value of the deep water phase speed. Now, let us introduce a *theoretical analogous of the finite depth wave age*, let say θ_{fd}

$$\theta_{fd} = \frac{1}{U_1} \sqrt{\frac{g}{k}} \sqrt{\tanh(kh)} = \theta_{dw} \sqrt{T}, \tag{31}$$

where $T = \tanh(\delta / \theta_{dw}^2)$.

The form (31) is a depth weighted parameter. For a given finite and constant θ_{dw} , note that if $\delta \rightarrow \infty$ then we have $\theta_{fd} \sim \theta_{dw}$ and if $\delta \rightarrow 0$ then $\theta_{fd} \sim \delta^{1/2} = \sqrt{gh} / U^2$. To obtain the growth rate, we introduce the following non-dimensional variables and scalings, hats stand for dimensionless quantities

$$U = U_1 \hat{U}, \quad W_a = W_0 \hat{W}_a, \quad z = \frac{\hat{z}}{k}, \quad c = U_1 \hat{c}, \quad t = \frac{U_1}{g} \hat{t}. \tag{32}$$

Using (30) and (32) in equation (26) and looking only at the terms of order one in ε we obtain \hat{c} ,

$$\hat{c}(\delta, \theta_{dw}) = \theta_{dw} T^{1/2} - \frac{\varepsilon}{2} \theta_{dw} T^{1/2} + \frac{\varepsilon}{2} \left\{ T \hat{I}_1 - \theta_{dw} T^{3/2} \hat{I}_2 \right\}, \tag{33}$$

and with

$$e^{\gamma t} = e^{k \Im(c) t} = e^{\Im(\hat{c}) \hat{t} / \theta_{dw}^2}, \tag{34}$$

we have the dimensionless growth rate $\hat{\gamma} = (U_1 / g) \gamma$ as,

$$\hat{\gamma} = \frac{\varepsilon}{2} \left\{ \frac{T \Im(I_1)}{\theta_{dw}^2} - \frac{T^{3/2} \Im(I_2)}{\theta_{dw}} \right\}. \tag{35}$$

Therefore, $\hat{\gamma}$ can be computed for a given set of (δ, θ_{dw}) . Since the parameter δ does not appear explicitly, it is possible to compute γ for an infinite depth, where $T \rightarrow 1$. This gives back the Miles' theory.

The unique curve of wave growth rate in deep water is transformed in a family of curves in the case of finite depth h indexed by $\delta = gh / U_1^2$, i.e., a curve for each value of δ . Fig. 1 shows a family of six values of δ against the θ_{fd} parameter. The limit $\delta \rightarrow \infty$ is included as well. Small finite θ_{fd} represents short surface waves. This stage corresponds the initial growth of the wave field near the shoreline of a calm sea. As the time proceeds the surface waves reaches moderate θ_{fd} corresponding to mild or moderate wavelengths, while long waves are found for large θ_{fd} . Of course, wavelengths and amplitudes increase together. This means that Fig. 1 is in fact, a snapshot of the theoretical dynamical development of the wave growing in amplitude and wavelength with time. The Fig. 1 shows also that for small θ_{fd} the values of δ does not influence the growth rate γ .

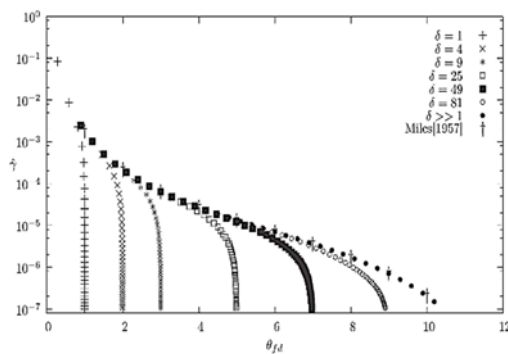


Fig. 1. Evolution of the growth rate in semilogarithmic scale. The six first curves from the left represent growth rates in finite depth. From left to right, they match $\delta = 1, 4, 9, 25, 49, 81$. Notice that for each depth, there is a θ_{fd} - limited wave growth. The deep water limit (the rightmost curve) also computed, corresponds to small θ_{fd} and matches Miles' results.

As θ_{fd} increases, the finite-depth effects begin to appear and for each value of δ , the growth rate becomes lower than in the deep water limit. The growth rates are scaled with δ : for a given θ_{fd} , the

bigger the δ is, the larger the $\hat{\gamma}$ will be. As $\hat{\gamma}$ goes to zero, each δ -curve approaches its own *theoretical θ_{fd} -limited growth*. At this stage the wave reaches the limit of its linear evolution. In other words, one can say that at this stage, for a given δ the surface wave does not grow older beyond a determined θ_{fd} .

In this paper, the analysis of the wind-wave growth is done through the dimensionless growth rate $\hat{\gamma}$. But usually, this is done with the help of β -Miles parameter. The relation between β and $\hat{\gamma}$ is

$$\beta = \frac{2\hat{\gamma}}{\varepsilon} \theta_{dw}^3 \sqrt{T}, \quad (36)$$

where β is defined as usually through the straight-forward definition of Miles' β in finite depth.

$$\mathfrak{F}(c) = c_0 \frac{\varepsilon}{2} \beta \left(\frac{U_1}{c_0} \right)^2. \quad (37)$$

Its evolution is shown clearly in Fig. 2 exhibiting the correct deep water trends, and the new finite depth limits. The effects of depth are critical. β is, as usual, almost constant for small θ_{fd} but it goes dramatically to zero when the depth limit is close.

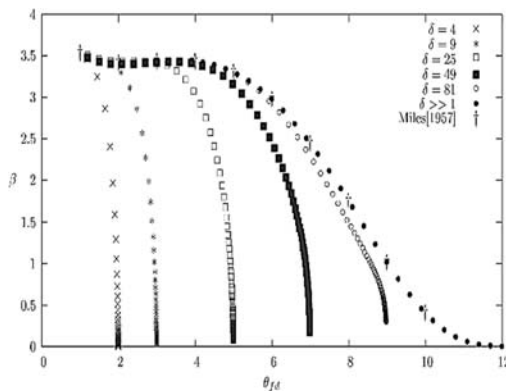


Fig. 2. Evolution of Miles' coefficient β for different values of the depth. All curves are plotted with the same Charnock constant $\alpha_c \approx 0.018$. The finite-depth effect is critical, and high values of δ correspond to deep water.

3. THEORETICAL LINEAR LAWS AND QUALITATIVE COMPARISONS WITH FIELD EXPERIMENTS

The pioneer experiments and numerical studies for the finite depth wave growth were conducted by (Thijssen, 1949), (Bretschneider, 1958), (Ijima and Tang, 2011) and in particular the experiments in Lake George, Australia, described by (Young and Verhagen, 1996a). This provides one of the first systematic attempts to understand the physics of wind generated waves in finite depth.

In the case of fetch limited growth, the results of the field experiments are presented in references (Young and Verhagen, 1996a) and (Young and Verhagen,

1996b). In these papers, we have a very complete description of bathymetry, basin geometry, experimental designs, experimental instrumentations, as well as the adopted scaling parameters. The measurements have confirmed the water depth dependence of the asymptotic behavior of wave growth.

An empirical relation in terms of appropriate dimensionless parameters able to reproduce the experimental data of (Young and Verhagen, 1996a) has been derived in references (Young, 1997a) and (Young, 1997b). In particular, it has been shown that for deep water, the fractional energy increases as a function of the inverse of wave age. Later (Donelan *et al.* 2006; Donelan, Babanin, Young, and Banner), this result has been extended to the finite depth domain. Experimental results together with empirical laws, show that contrary to the deep water case, the wave age at which the growth rate becomes zero (limit of the linear behavior) is both wind and depth-dependent. Therefore, the point of full development is warped from the deep water case (Pierson and Moskowitz, 1964). Consequently, a growth law as a function of the inverse of the wave age exists for each value of a parameter including the dependences on wind intensity and water depth.

Concerning the evolution of the growth rates, one can say that for small wave ages, growth rates are comparable to the deep water limit, and for large wave ages, the growth rate is lower in shallow water than in deep water. Moreover, beyond a limit wave age, the growth rate vanishes.

3.1 Comparisons With Field Experiments

In this subsection, it will be shown that our analytical and numerical results are able to qualitatively reproduce these experimental facts. At this point, we have to keep in mind that our study is based on linear growth of a normal Fourier mode k and not the growth of a wave train as an infinite superposition of wave Fourier modes.

Moreover, given results in field or laboratory experiments usually uses the parameter C_p , the observed phase speed at the peak frequency ω_p . As a result, qualitative comparison with field observations can only be done using the phase velocity c or frequency ω of one mode instead of C_p or ω_p .

At first, let us show that the theoretical curves for $\hat{\gamma}$ are in good qualitative agreement with the empirical curves corresponding to the increase per radian of the dimensionless fractional wave energy $\hat{\Gamma}$ as a function of the inverse of wave age U_{10}/C_p obtained by (Young, 1997a). In this reference, experimental field data for $\hat{\Gamma}$ in the finite depth Lake George are adequately represented by the empirical relationship

$$\hat{\Gamma} = \frac{C_g}{\omega_p} \frac{1}{E} \frac{\partial E}{\partial x} = A \left(\frac{U_{10}}{C_p} - 0,83 \right) \tanh^{0,45} \left(\frac{U_{10}}{C_p} - \frac{1,25}{\delta_Y^{0,45}} \right), \quad (38)$$

with A constant, $\delta_Y = gh / U_{10}^2$ the non-dimensional water depth, U_{10} the wind velocity at 10 m, and C_g and C_p the group and phase speeds of the components at the spectral peak frequency ω_p .

To be able to make a qualitative comparison between $\hat{\Gamma}$ curves (in function of the inverse wave-age U_{10}/C_p) and theoretical $\hat{\gamma}$ curves (in function of $1/\theta_{fd}$), it is necessary to write the empirical $\hat{\Gamma}$ in terms of theoretical quantities. So, we will have to transform the measured quantities C_g, C_p, ω_p into theoretical g, c, ω quantities and put

$$\frac{U_{10} C_{10}^{1/2}}{k} = u_* / \kappa = U_1 \quad (39)$$

with C_{10} the drag coefficient at 10 m (Wu(1982)). Then, using $\Gamma = 2\gamma, 2c_g = c(1 + 2kh / \sinh(2kh))$, (39), (31) and (32) we obtain

$$\hat{\Gamma} = \frac{\theta_{dw}}{\sqrt{T}} \hat{\gamma} \left\{ 1 + \frac{2\delta}{\theta_{dw}^2} \sinh^{-1} \left(\frac{2\delta}{\theta_{dw}^2} \right) \right\}. \quad (40)$$

This expression provides the theoretical equivalent of the empirical $\hat{\Gamma}$ in function of, δ and $\hat{\gamma}$. The values of $\hat{\gamma}$ for fixed δ 's as a function of $1/\theta_{dw}$ are numerically obtained from Eqs. (31) (??) and (35) and (39) transforms δ_Y and C_p / U_{10} into δ and θ_{fd} according to

$$\delta_Y = \delta C_{10} \kappa^{-2}, \frac{C_p}{U_{10}} = \theta_{fd} (C_{10})^2 \kappa^{-1}. \quad (41)$$

In reference (Young, 1997a) the curves of Γ versus U_{10}/C_p have been presented for the δ_Y - intervals $\delta_Y \in [0.1 - 0.2], [0.2 - 0.3], [0.3 - 0.4], [0.4 - 0.5]$, rather than for a single value of δ_Y . The intervals were determined from the variations in U_{10} and the depth h nearly constant around 2 m. Using (41), we substitute the δ_Y - intervals by δ -intervals and we evaluate the mean value $\bar{\delta}$. For instance, in Fig. 3 (a), $\delta_Y \in [0,1 - 0,2]$ is transformed into $\delta = [13,17 - 26,35]$ with $\bar{\delta} = 19,76$. Figs. 3(a), 3(b), 3(c) and 3(d) display a fair concordance between the model and the experimental data and plots of empirical laws for Lake George. The agreement improves as $1/\theta_{fd}$ increases.

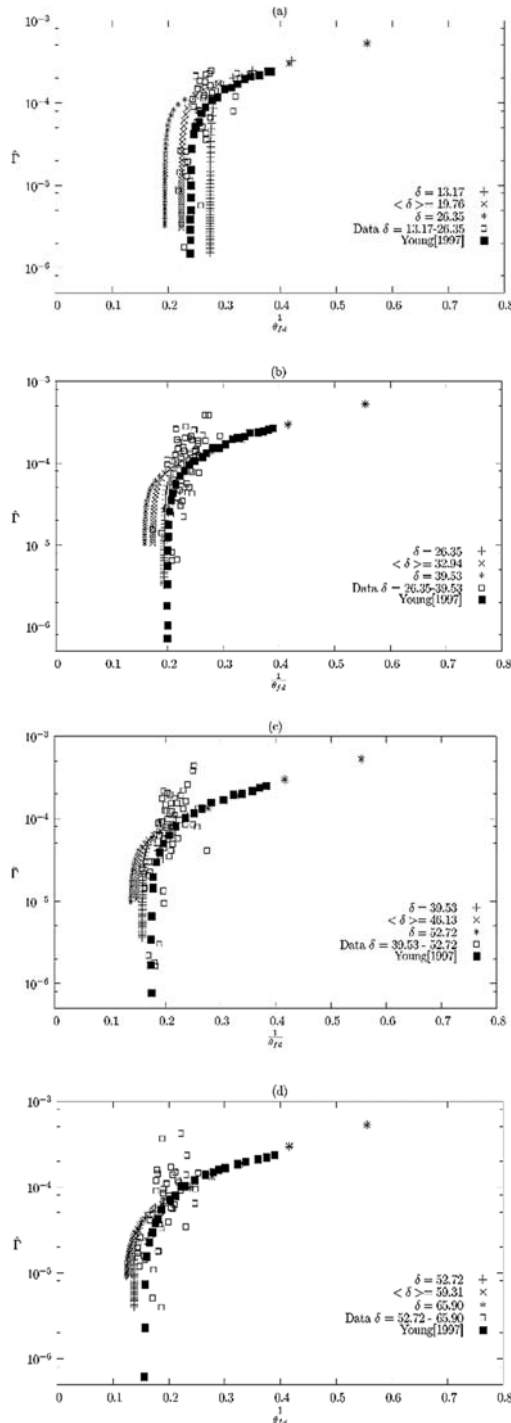


Fig. 3. Growth rate $\hat{\Gamma}$ as a function of inverse wave age $1/\theta_{fd}$ for different values of δ . White squares correspond to Lake George experiment data, Black squares correspond to the empirical relationship found by (Young, 1997a). Present results are represented by the symbols +, × and *. a: the dataset covers a range of wind speed corresponding to $\delta_Y = 0.1-0.2$, or using (41) $\delta=13.17-26.35$, and an average value $\langle \delta \rangle = (13.17 + 26.35)/2$. b: same as “a” with $\delta_Y = 0.2 - 0.3$. c: same as “a” with $\delta_Y = 0.3-0.4$. d : same as “a” with $\delta_Y = 0.4-0.5$.

In Fig. 4 are plotted, against δ , the critical values of the parameter θ_{fd}^c for which the growth rate γ goes to zero, obeying $\theta_{fd}^c = \delta^{0.5}$. This relation, found numerically, is coherent with the parameter formulation (31). It is indeed a limiting value for θ_{fd} uniquely determined by the water depth. In (Young, 1997a) the author has shown from an empirical relationship (formula (6) in reference above) that Γ the growth rate goes to zero as a function of the inverse wave age U_{10}/C_p fo

$$\frac{C_p}{U_{10}} = 0.8 \left(\frac{gh}{U_{10}^2} \right)^{0.45} \quad (42)$$

Choosing a C_{10} drag coefficient parametrization such as (Wu(1982))

$$C_{10} = (0.065U_{10} + 0.8)10^{-3}, \quad (43)$$

and taking an average $U_{10} = 7m/s$ in (Young(1997a)), one finds the relation between U_1 and U_{10}

$$U_{10} \approx 28,3u_* \approx 11,6U_1, \quad (44)$$

So, this limiting law reads

$$\frac{C_p}{U_1} = 1,01\delta^{0,45}. \quad (45)$$

The parameter θ_{fd}^c allows the calculation of the corresponding critical Awave length λ^c . Using (31) yields to

$$\delta\theta_{dw}^{-2} = \tanh\left(\delta\theta_{dw}^{-2}\right). \quad (46)$$

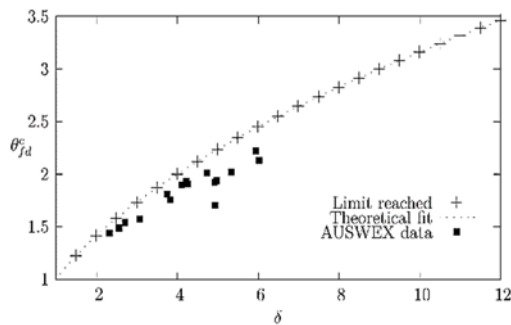


Fig. 4. Parameter curves corresponding to zero growth rate. The theoretical limit is given $\theta_{fd}^c = \delta^{0.5}$. The AUSWEX data are experimental results (Donelan *et al.*(2006)Donelan, Babanin, Young, and Banner) (the sea state is fairly close to the finite depth full development).

From the physical point of view, the relation (46) means the wave has entered the shallow water region. In such a limit

$$0 < \delta\theta_{dw}^{-2} < \frac{\pi}{4} \quad ((\text{Fenton, 1979}), (\text{Francius and$$

Kharif, 2006)). This gives $\lambda^c = 8h$. For $\lambda > \lambda^c$ the

phase velocity is in the long wave limit i.e., $c = \sqrt{gh}$. Consequently, if $\lambda > \lambda^c$ the wave feels the bottom, the amplitude does not grow anymore, the resonance wind/phase speed ceases, and the wave reaches its utmost state as a progressive plane wave.

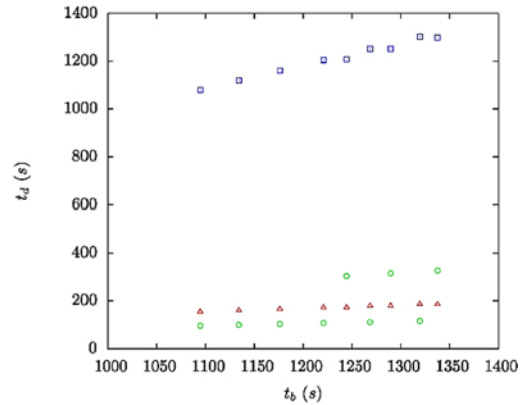


Fig. 5. Comparison of velocity (triangles), Miche (circles) and McCowan (squares) criteria. Plotted are the trends for the allowed values of t_d, t_b , with $\nu = 1/10$. The breaking time, always inferior to the blow-up time, are very closed to eac other with the McCowan criterion. The Miche and velocity criteria give both breaking times of similar order

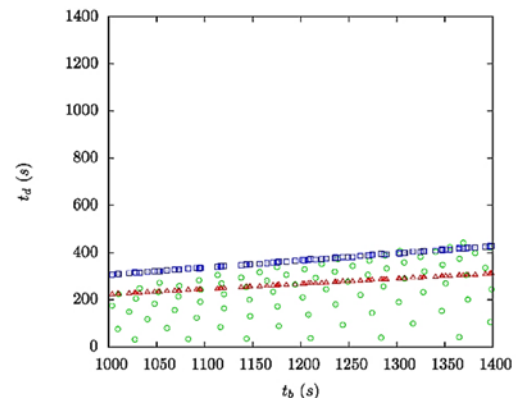


Fig. 6. Same as in Fig. 5 with $\nu = 1/3$. the wave velocity criterion is represented by triangles, Miche by circles and McCowan above, with squares. The higher amplitude yields shorter breaking times for McCowan and Miche, and a wider range of allowed values for the parameters. There is a higher scatter in the Miche criterion.

Finally in Fig. 4 are also represented data from (Donelan *et al.* 2006) Donelan, Babanin, Young, and Banner), from the Australian Shallow Water Experiment. A fit is also plotted to show the trend. The raw data consists in the water depth h in meters, the friction velocity u_* , the 10 meters wind velocity U_{10} and the ratio of the former with the measured phase speed c_p , U_{10}/c_p . For example,

$u_* = 0.44 m s^{-1}$ and $h = 0.32 m$ gives $\delta = 2.7$ and $\theta_f d = 1.55$, and corresponds to a small relative error. All the points give (δ, θ_{fd}) coordinates are closed to the theoretical limit.

3.2 The White-Capping Dissipation Influences

The aim of this subsection is to answer the question: why do the $\hat{\Gamma}$ curves seem to be consistent with the empirical fits of (Young, 1997a) in spite of the fact that bottom friction dissipation S_{bf} and white-capping dissipation S_{ds} are disregarded. It is commonly admitted that the bottom friction S_b plays a relatively minor role in depth limited growth studies, even though being an important dissipative factor for swell propagating in shallow water (Young and Babanin, 2006b). Since in finite depth, wind waves show significant wave breaking events, the white-capping dissipation S_{ds} is considered to be the dominant dissipative term compared to the deep water case (Young and Verhagen, 1996a); Young and Babanin, 2006b). Now, let us review what can be observed in plots 3(a), 3(b), 3(c) and 3(d).

- For young sea regimes ($1/\theta_{fd}$ large), it can be seen in Figs. 3(a), 3(b), 3(c) and 3(d) that the $\langle \delta \rangle$ -curves match the experimental $\hat{\Gamma}_Y$ (in black squares) which means that in these regimes $\hat{\Gamma} = \hat{\Gamma}_Y$. Small values of θ_{fd} correspond to wave propagating in deep water, for any $\langle \delta \rangle$. This is in agreement with Fig. 7.1.c in (Young, 1997b) where S_{ds} tends to zero for large frequencies.
- For mature or old sea regimes ($1/\theta_{fd}$ small) both curves $\hat{\Gamma}$ and $\hat{\Gamma}_Y$ vanish. In developed finite depth seas, the evolution of the wave energy (amplitude) becomes depth limited independently from the value of S_{ds} . Therefore, the finite depth-limitation phenomenon prevails.
- For intermediate regimes the $\hat{\Gamma}$ and $\hat{\Gamma}_Y$ curves have similar shapes. Nevertheless, $\hat{\Gamma} > \hat{\Gamma}_Y$ for all the values of $\langle \delta \rangle$. This is in agreement with Fig. 7.1.c in (Young, 1997b) where $S_{ds} \leq 0$ for intermediate frequencies. Hence, the wave growth rate $\hat{\gamma}$ is overestimated in our model. One can see in Figs. 3(a), 3(b), 3(c) and 3(d) that the gap between $\hat{\Gamma}$ and $\hat{\Gamma}_Y$ increases as $\langle \delta \rangle$ decreases, because the white-capping S_{ds} is larger and wider for small kh in accordance with Fig. 7.1.c in (Young, 1997b).

4. THE NONLINEAR SURFACE WAVES REGIME

4.1 Nonlinear Jeffrey' approach In Jeffreys' theory (Jeffreys, 1925); Jeffreys, 1926) once again, one supposes both the water as and the air to be inviscid,

incompressible and obeying to linearized equations of motion. This theory allows to calculate the linear wave growth of wind-generated normal Fourier modes of wave-number k . The underlying physical mechanism is anti-dissipation. In this mechanism, energy passes continuously from the air to the surface wave. Consequently the wave amplitude $\eta(x,t,k)$ grows exponentially in time; $\eta(x,t,k) \sim \exp(\gamma_J t)$ more or less quickly according to the coefficient γ_J , which depends on the wind speed and the water depth h . The nonlinear and dispersive processes begin to play a role, once the linear dispersionless approximation breaks down. Now, the question we rise is: how to describe the time evolution of a normal mode k , under the competing actions of (weak) nonlinearity, dispersion and antidissipation? Nonlinearity is likely to balance dispersive effects, or to stop exponential time evolution of wave amplitude due to dissipation or anti-dissipation. Balance between nonlinearity and dispersion can evolve in time and end up to solitary waves as in the Korteweg-de Vries equation (Whitham, 1974); Korteweg and de Vries, 1895). Equilibrium between dissipation or anti-dissipation and nonlinearity creates shock structures as in the Burgers equation (Whitham, 1974). And finally the standard equation describing competition between weak non-linearity, dispersion and dissipation is the Korteweg-de Vries-Burgers equation (KdV-B) which appears in many physical contexts (see (Benney, 1996), (Johnson, 1972), (Grad and Hu, 1967); Hu, 1972), (Wadati, 1975), (Karahara, 1970). In this section, in order to study simultaneous competing effects of weakly nonlinearity, dispersion and anti-dissipation we derive a KdV-B type equation with dissipation turned into anti-dissipation.

4.2 Derivation of the Anti-Diffusive Korteweg-De Vries-Burger Equation

In this section, we consider a quasi-linear air/water system with the air dynamics linearized and the water dynamics seen as nonlinear and irrotational. As previously, the system is $(2 + 1)$ dimensional (x,z,t) with x and z the vertical and the horizontal space coordinates. The aerodynamic air pressure $P_a(x,z,t)$ evaluated at the free surface $z = \eta(x,t)$ has a component in phase and a component in quadrature with the water elevation. To have an energy transfer from the wind to the water waves, there must be a phase shift between the fluctuating pressure and the interface. Therefore, the energy flux is due to the component in quadrature with the water surface, or in other words in phase with the slope. To simplify the problem, following references (Jeffreys, 1926), (Miles, 1957) (Kharif *et al.* 2010) Kharif, Kraenkel, Manna, and Thomas), we consider only the pressure component in phase with the slope on the interface i.e.,

$$P_a = s \rho_a \Delta^2 \frac{\partial \eta}{\partial x} \text{ with } \Delta = \kappa U_1 C_{10}^{-1/2} - c \quad (47)$$

where $s < 1$ is the sheltering coefficient. This is nothing more than Jeffrey's sheltering mechanisms. Now, let us introduce dimensionless primed

variables: $x = lx'$, $z = hz'$, $t = lt' / c_0$, $\eta = a\eta'$, $\phi = gla\phi' / c_0$, $U_1 = c_0 U_1'$ with ϕ the velocity potential and a and l typical wave amplitude and wavelength and $c_0 = \sqrt{gh}$. Let us define two dimensionless parameters too $v = a/h < 1$ and $\delta = h/l < 1$. So then, the complete irrotational Euler equations and boundary conditions are (dropping the primes)

$$\delta^2 \frac{\partial^2 \phi}{\partial x^2} + \frac{\partial^2 \phi}{\partial z^2} = 0, \text{ for } -1 < z < v\eta, \quad (48)$$

$$\frac{\partial^2 \phi}{\partial z^2} = 0, \text{ for } z = -1, \quad (49)$$

$$\frac{\partial \eta}{\partial t} + v \frac{\partial \phi}{\partial x} \frac{\partial \eta}{\partial x} - \frac{1}{\delta^2} \frac{\partial \phi}{\partial z} = 0, \text{ for } z = v\eta, \quad (50)$$

$$\frac{\partial \phi}{\partial t} + \frac{v}{2} \left(\frac{\partial \phi}{\partial x} \right)^2 + \frac{v}{2\delta^2} \left(\frac{\partial \phi}{\partial z} \right)^2 + \eta + \eta \delta \varepsilon \Delta^2 \frac{\partial \eta}{\partial x} = 0, \text{ for } z = v\eta, \quad (51)$$

where, as defined previously, $\varepsilon = \rho_a / \rho_w \sim 10^{-3}$. We solve the Laplace equation and its boundary conditions with an expansion in powers of $(z + 1)$,

$$\phi = \sum_{m=0}^{m=\infty} (z + 1)^m \delta^m q_m(x, t). \quad (52)$$

Substituting in Eq. (48) and using Eq.(49) we obtain

$$\phi = \sum_{m=0}^{m=\infty} (-1)^m \frac{(z + 1)^{2m}}{(2m)!} \delta^{2m} \frac{\partial q_{0,2m}}{\partial x}. \quad (53)$$

Using the kinematic and dynamics boundary conditions (50), (52) and disregarding terms in $O(v \delta^2)$ and $O(\delta^4)$, we find with $r = \partial_x q_0$, the following system

$$\frac{\partial \eta}{\partial t} + \frac{\partial \{(1 + v\eta)r\}}{\partial x} - \frac{1}{6} \delta^2 \frac{\partial^3 r}{\partial x^3} = 0, \quad (54)$$

$$\frac{\partial \eta}{\partial x} + \frac{\partial r}{\partial t} + vr \frac{\partial r}{\partial x} - \frac{1}{2} \delta^2 \frac{\partial^3 r}{\partial x^2 \partial t} + \delta \varepsilon \Delta^2 \frac{\partial^2 \eta}{\partial x^2} = 0. \quad (55)$$

The linear wave solution of (54) and (55) moving to the right is $r(x - t) = \eta(x - t)$, with η (or r) an arbitrary function of $x - t$. Now we look for a solution with nonlinear corrections to the orders $O(v)$, $O(s\delta)$, and $O(\delta^2)$. Following the procedure in reference (Whitham, 1974) yields

$$r = \eta - \frac{1}{4} \eta^2 v + \frac{s}{2} \Delta^2 \frac{\partial \eta}{\partial x} \varepsilon \delta + \frac{1}{3} \delta^2 \frac{\partial^2 \eta}{\partial x^2} + O(v\delta^2, \varepsilon^2 \delta^2, \delta^4), \quad (56)$$

Substituting (56) in (54) and (55) we obtain the anti-dissipative KdV-B equation

$$\frac{\partial \eta}{\partial t} + \frac{\partial \eta}{\partial x} + \frac{3}{2} v \eta \frac{\partial \eta}{\partial x} + \frac{1}{6} \delta^2 \frac{\partial^3 \eta}{\partial x^3} + \frac{3}{2} \delta s \Delta^2 \frac{\partial^2 \eta}{\partial x^2} = 0. \quad (57)$$

For traveling wave solutions, the action of dissipation or anti-dissipation in KdV-B is not of great matter except for the sign of the slope (Jeffrey and Xu, 1989). But the important fact is that soliton solutions under anti-dissipation exhibits a blow-up and breaking in finite time.

4.3 Blow-up and breaking of solitary waves in finite time In the usual KdV-B equation the effect of (weak) dissipation, for instance through bottom friction, is to decrease slowly the amplitude and to increase slowly the width of the solitary wave solution, eventually flattening it in an infinite time. In our case, anti-diffusion increases the soliton amplitude and decreases the width of the solitary wave solution. In opposite of the diffusive KdV-B equation which dissipates energy in time here the wave energy grows in time. Multiplying (57) by $\eta(x, t)$, assuming the limit $\eta(\pm\infty, t) = 0$ and integrating over the x -axis, we obtain

$$\frac{\partial}{\partial t} \int_{-\infty}^{\infty} \eta^2 dx = \frac{\varepsilon}{4} \delta s \Delta^2 \int_{-\infty}^{\infty} \left(\frac{\partial \eta}{\partial x} \right)^2 dx. \quad (58)$$

Since the right hand side is positive definite, the wave energy $E = \int_{-\infty}^{\infty} \eta^2 dx$ monotonically increases in time. In KdV we must have balance between nonlinearity and dispersion i.e. $O(v) \sim O(\delta^2)$. And if we assume the dissipative effects to be weaker than the dispersive and nonlinear effects, then we have $(s/2) \delta \varepsilon \Delta^2 \sim O(\delta^3)$.

The validity of above hypothesis is checked by evaluating typical values of Δ for reasonable wind speed (not higher than 20 m/s). In these conditions and after a Galilean transform in order to eliminate the term $\partial_x \eta$, an approximate solution of Eq. (57) is given by (see reference (Ott and Sudan, 1970) for the dissipative case)

$$\eta = a(t) \cosh^{-2} \left[\frac{\alpha}{\sqrt{\alpha(t)}} \left[x - t - \frac{v}{2} \int^t (t') dt' \right] \right] \quad (59)$$

with $\alpha^2 = 3v/4\delta^2$ and $a(t)$ the time-dependent amplitude given by

$$a(t) = \left[1 - \frac{t}{t_b} \right]^{-1}, \quad (60)$$

where t_b is the blow-up time which can be written in terms of the system parameters as

$$t_b = \frac{5\delta}{2s\varepsilon\Delta^2 v}. \quad (61)$$

$$\theta(x, t) = \alpha \left(1 - \frac{t}{t_b} \right)^{-\frac{1}{2}} \left[x - t + \frac{vt_b}{2} \ln \left(1 - \frac{t}{t_b} \right) \right]. \quad (62)$$

As t approaches t_b , $\eta \rightarrow 0 \forall x$ except for $x \rightarrow +\infty$ as $\lim_{t \rightarrow t_b} [t - (vt_b/2)\ln(1 - t/t_b)]$. So at $x(t_b) \rightarrow +\infty$ the model presents an x -asymptotic blow-up in finite time. This is a nonlinear, dispersive and anti-dissipative instability analogous to the linear, anti-dissipative instability in the Jeffreys' approach: the solitary wind-wave replaces the plane-wave and the blow-up $x(t_b) \rightarrow +\infty$ in finite time $t = t_b$ replaces the local wave-amplitude divergence in infinite time.

Obviously, for $t = t_b$ the model breaks down. But before $t = t_b$, the model gives an accurate kinematic and dynamic description of the route to breaking of solitary wind-waves.

For large t , higher-order nonlinear, dispersive and dissipative effects will appear. However, our model (57) is of order 3 in δ , hence the longest allowed time τ has to be $\tau = \delta^3 t$, which is of order unity for large t , such as $t_b \propto \delta^{-3}$. In order to be sure of the model validity, we have checked that the derivatives of η in (57) stayed of order unity when $t < t_b$.

4.4 Wave Breaking Criteria

Clearly, the soliton blow-up is impossible to probe experimentally. To resolve this problem, an interesting approach is to evaluate the breaking time t_d of the solitary wave under this specific wind forcing (before the blow up). The breaking time, and more generally breaking conditions, have been subject to many discussions. Determine effective criteria of breaking has been an important center of interest in the literature. Here, we study three of the most widely known effective breaking criteria. Our goal is to compare t_d with t_b as given by (61).

The first one is the McCowan criterion (Mc-Cowan, 1894). It is reached for a limiting ratio of the maximum wave height a_{max} and the water depth h given by $a_{max}/h \approx 0.78$.

The second is the Miche criterion (Miche, 1944). It regards the limiting wave slope a/λ . Breaking occurs for

$$\left(\frac{a}{\lambda}\right)_{max} = \frac{1}{7} \tanh\left(\frac{2\pi h}{\lambda}\right). \tag{63}$$

For the soliton solution, the time-dependent value λ is interpreted as an effective wavelength. In laboratory variables, it depends only on the water depth h and wave height a ; $\lambda = 2\pi\sqrt{4h^3/3a}$. Of course, a still time-dependent.

The third is the wave horizontal velocity criterion (velocity criterion for short, (Shemer, 2013). When the horizontal speed r exceeds the speed of the phase plane at the crest i.e. $r > c$ matter starts to be ejected from the wave, and breaking can appear. r is obtained from (56). This third criterion depends directly on kinematics of the problem, and is exempt of the empirical aspect of the two other laws. Hence, we

obtain the corresponding breaking time by perturbation for the velocity criterion $t_d = 1.25 t_b v + O(v^{3/2})$. Each of these three

criteria gives a different breaking time t_d , which is plotted in order to be compared to t_b . We took at ranges of $U_{10} \in [4;22]$ m/s for the wind, and $h \in [0.1;4]$ m. The results are shown in Fig. 5 and Fig. 6.

For $v = 1/10$, the highest values of t_d belongs to McCowan criterion, the Miche criterion has a too big spread depending on the input parameters to be accurate and as one can see, the shortest time breaking values belongs to the velocity criterion. In Fig. 6, the parameter value is taken to be $v = 1/3$. We have have check that v and δ are of same order. But of course, we cannot change the value of ϵ (the air to water density ratio). Therefore, in order to keep the balance between terms in (57), we have to consider higher Δ which corresponds to strong winds values up to $U_{10} \approx 20$ (m/s). In this context, there is no drop of the drag coefficient (Makin, 2004), and consequently no foam formation. Therefore, the derived KdV-B equation is still valid. In this case, the McCowan criterion gives lower values for the breaking time t_d and an even larger spread for the Miche criterion. One can see that the velocity criterion gives analogous values of t_d than in the $v = 1/10$ case. The kinematic criterion is more stable than the others with respect to parameter variations, so we can consider this criterion to be the most relevant for our study.

4.5 Kinematics Description of Wind-Solitary Wave Breaking.

The phase θ defines a local wave number $k = \partial\theta/\partial x$ and a local frequency $\omega = -\partial\theta/\partial t$, therefore the local phase velocity $c = \omega/k$ is

$$c(x,t) = 1 + \frac{v}{2} a(t) - \frac{\theta(x,t)\sqrt{a(t)}}{2\alpha t_b}. \tag{64}$$

We have also a local phase acceleration

$$\gamma(x,t) = \frac{a(t)}{t_b} \left[\frac{1}{2} + \frac{3}{4} v a(t) - \frac{\sqrt{a(t)}\theta(x,t)}{2\alpha t_b} \right]. \tag{65}$$

The constant phase planes $\theta(x,t) = \theta_0$ moves with velocities $c(\theta_0,t)$ and acceleration $\gamma(\theta_0,t)$. It worth remarking that, two planes θ_1 and θ_2 around a given θ_0 (for example the soliton maximum), such that $\theta_1 < \theta_0 < \theta_2$ have speeds and accelerations in the opposite ordering; $c(\theta_1,t) > c(\theta_2,t)$ and $\gamma(\theta_1,t) > \gamma(\theta_2,t)$. This phenomenon destroys the soliton symmetry and brings to breaking for $t \rightarrow t_d$.

4.6 Prospect of an Experimental Test

In this subsection we will show that the theoretical

amplitude growth and the of breaking time are both testable in the existing experimental facility.

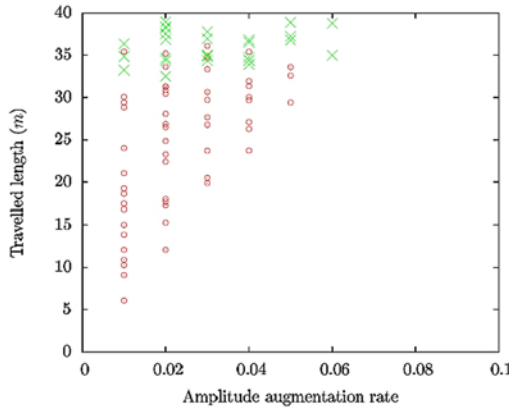


Fig. 7. In a 40-meters long wind tunnel, this plotted shows at what point and which time a certain growth rate is attained. Circles exhibit a time $t < 10$ s, and on the upper part in crosses correspond to $t \geq 10$ s. The values are computed for different constant depths between 0.7 and 1.0 meters, a reference wind speed $U_{10} < 15$ m/s, and a wave steepness $ka > 0.23$. In these conditions, the growth rate can be more than 6%.

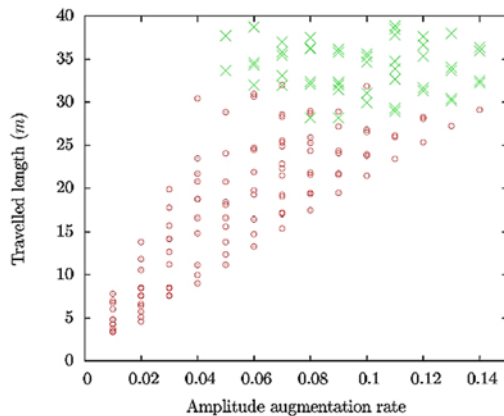


Fig. 8. Same as in Fig.7 with the ranges of wind and depth $0.3 \text{ m} \leq h \leq 0.7 \text{ m}$, the reference wind speed $15 \text{ m/s} < U_{10} < 20 \text{ m/s}$, and the wave steepness $ka > 0.23$. circles correspond to $t < 10$ s, and crosses to $t \geq 10$ s. These conditions allow a much greater energy transfer and a significantly faster growth. The amplitude increases by up to 15% within the tunnel length.

The Jeffreys mechanism acts only on waves steep enough to shelter the front side from the wind. Typically, a steepness parameter $ka > 0.3$ is necessary (Montalvo *et al.* 2013a) Montalvo, Dorignac, Manna, Kharif, and Branger; Montalvo *et al.* 2013b)Montalvo, Kraenkel, Manna, and Kharif). But, we can see that at $t = 0$, (59) is too smooth to allow sheltering. Therefore, to have a steep enough soliton, setting $v = 1/3$ is necessary. In these

conditions, we define t_n , the time taken by the maximum amplitude of the soliton solution to grow of $n\%$. We have $t_n = nt_b / (n + 1)$. If we assume that the soliton is created in a 40-meters long wind tunnel which can be filled up to 1 m of water depth, it allows then to evaluate in these conditions what would be the rise of the soliton. The results are shown in Figs. 7 and 8. Those results show that a fair augmentation of the soliton amplitude can be measured before the end of the tunnel. This shows this model, it is indeed possible to confront the measured amplitude increase time to the theoretical one.

4.7 The Anti-Diffusive Nonlinear Schrödinger Equation in Finite Depth

Now, we are going to consider the wind effects via the Miles’s mechanism and instead of studying the wind action on a single Fourier wave-number k , we study its action on a wave packet. We take the β -Miles parameter as given by expression 36.

In Miles’s theory of wave generation (Miles, 1957), the complex air pressure P_a can be separated into two components, one in phase and the other in quadrature with the free surface η . A phase shift between these two quantities is necessary to transfer energy from the air flow to the wave field. The transfer is only due to the part of P_a in quadrature with η . Hence, we will deal only with the acting pressure component, that is

$$P_a(x, t) = \rho_a \beta U_1^2 \frac{\partial \eta(x, t)}{\partial x}. \tag{66}$$

Let us consider the air/water system from a quasi-linear point of view. Namely, the water dynamics is considered nonlinear and irrotational and, as in Miles’ theory, the air flow is kept linear. With this assumptions, the complete irrotational Euler equations and boundary conditions in terms of the velocity potential $\phi(x, z, t)$ are

$$\frac{\partial^2 \phi}{\partial x^2} + \frac{\partial^2 \phi}{\partial z^2} = 0, \text{ for } -h \leq z \leq \eta, \tag{67}$$

$$\frac{\partial \phi}{\partial z} = 0, \text{ for } z = -h, \tag{68}$$

$$\frac{\partial \eta}{\partial t} + \frac{\partial \phi}{\partial x} \frac{\partial \eta}{\partial x} - \frac{\partial \phi}{\partial z} = 0, \text{ for } z = \eta, \tag{69}$$

$$\frac{\partial \phi}{\partial t} + \frac{1}{2} \left(\frac{\partial \phi}{\partial x} \right)^2 + \frac{1}{2} \left(\frac{\partial \phi}{\partial z} \right)^2 + g\eta = -\frac{1}{\rho_w} P_a, \tag{70}$$

for $z = \eta$,

Using (66), the modified Bernoulli equation reads

$$\frac{\partial \eta}{\partial t} + \frac{1}{2} \left[\frac{\partial \phi}{\partial x} \right]^2 + \frac{1}{2} \left[\frac{\partial \phi}{\partial z} \right]^2 + g\eta = -s\beta(U_1)^2 \frac{\partial \eta}{\partial x} \text{ for } z = \eta \tag{71}$$

From Eqs. (67), (68), (69) and (71) we find a wind-

forced finite depth NLS equation for η as a function of the standard slow space $\xi = \varepsilon(x - c_g t)$ and slow time $\nu = \varepsilon^2 t$ variables ($\varepsilon \ll 1$) and c_g the group velocity. The perturbed NLS equation reads

$$i \frac{\partial \eta}{\partial \nu} + a \frac{\partial^2 \eta}{\partial \xi^2} + b |\eta|^2 \eta = id \eta. \quad (72)$$

The coefficients c_g, a, b and d are given explicitly at the end of the paper, in (Section B). For more information about the derivation of these coefficients see (Thomas *et al.* 2012) Thomas, Kharif, and Manna).

To derive a dimensionless wind-forced NLS equation we use (32). In the original laboratory variables x and t (after a Galilean transformation in order to eliminate the linear term $c_g \eta_x$ and dropping the hats), we have

$$i \frac{\partial \eta}{\partial t} + A \frac{\partial^2 \eta}{\partial x^2} + B |\eta|^2 \eta = iD \eta \quad (73)$$

The coefficients c_g, A, B , and D are given explicitly at the end of the paper, in (Section B).

Equation (73) is a wind-forced finite depth NLS equation in dimensionless variables.

4.8 The Akhmediev, Peregrine and Ma Solutions for Weak Wind Inputs in Finite Depth

The classical nonlinear Schrödinger equation provides a model for freak waves, see for instance (Touboul and Kharif, 2006); Touboul *et al.* 2008) Touboul, Kharif, Pelinovsky, and Giovanangeli; Kharif *et al.* 2008; Kharif, Giovanangeli, Touboul, Grade, and Pelinovsky). The wind-forced nonlinear Schrödinger equation allows the study of the wind influence on the freak waves dynamics (Touboul and Kharif, 2006; Touboul *et al.* 2008) Touboul, Kharif, Pelinovsky, and Giovanangeli; Kharif *et al.* 2008) Kharif, Giovanangeli, Touboul, Grade, and Pelinovsky; Onorato and Proment, 2012). These authors have carried out their studies in deep water. The present work allows, similar studies in finite depth with the right Miles' growth rates. In this work, we consider the so called focusing NLS equation i.e. positives A and B . Introducing $\eta' = \sqrt{B} \eta$ and $x' = x / \sqrt{A}$. Then the Eq. (73) transforms, dropping the primes, into

$$i \frac{\partial \eta}{\partial t} + \frac{\partial^2 \eta}{\partial x^2} + |\eta|^2 \eta = iD \eta \quad (74)$$

Introducing a function $M(x,t) = \eta(x,t) \exp(-Dt)$, we obtain from (74)

$$i \frac{\partial M}{\partial t} + \frac{\partial^2 M}{\partial x^2} + \exp(2Dt) |M|^2 M = 0. \quad (75)$$

In order to reduce Eq. (74) into the standard form

of the NLS (with constant coefficients), we apply the following steps. First, we consider the wind forcing $2Dt$ to be weak, so the exponential can be approximated by $\exp(-2Dt) \sim 1 - 2Dt$ which yields

$$i \frac{\partial M}{\partial t} + \frac{\partial^2 M}{\partial x^2} + n |M|^2 M = 0, \quad n = n(t) = 1 - 2Dt. \quad (76)$$

Then we apply the change of coordinates from (x,t) to (z,τ) defined by $z(x,t) = xn(t)$ and $\tau(x,t) = xn(t)$. Finally by scaling the wave envelope as (Onorato and Proment, 2012)

$$M(z,\tau) = \Psi(z,\tau) \sqrt{n(\tau)} \exp \left[\frac{-iDz^2}{n(\tau)} \right], \quad (77)$$

we reduce (76) to the standard focusing Eq.

$$i \frac{\partial \Psi}{\partial \tau} + \frac{\partial^2 \Psi}{\partial x^2} + |\Psi|^2 \Psi = 0. \quad (78)$$

Eq. (78) admits the well known breather solutions that are simple analytical prototypes for rogue wave events. There are the Akhmediev (Ψ_A) (Akhmediev *et al.* 1987) Akhmediev, Eleonskii, and Kulagin), the Peregrine (Ψ_p) (Peregrine, 1983) and the Kuznetsov-Ma (Ψ_M) (Ma, 1979) breather solutions.

(Dysthe and Trulsen, 1999) investigated whether freak waves in deep water could be modeled by Ψ_A , Ψ_p or by Ψ_M . (Onorato and Proment, 2012) considered the influence of weak wind forcing and dissipation on Ψ_A , Ψ_p , Ψ_M solutions in deep water. The present work allows to exhibit expressions for Ψ_A , Ψ_p and Ψ_M under the influence of weak wind in finite depth h given by the extended Miles mechanism. These solutions read (Dysthe and Trulsen, 1999):

$$\eta_A = \frac{\cosh(\Omega \tau - 2i \omega) - \cos(\omega) \cos(qz)}{\cosh(\Omega \tau) - \cos(\omega) \cos(qz)} P(\tau) \quad (79)$$

with $q = 2 \sin(\omega)$, $\Omega = 2 \sin(2\omega)$ ω real and q related to the spatial period $2\pi/q$

$$\eta_p = \left\{ 1 - \frac{4(1 + 4i \tau)}{1 + 4z^2 + 16\tau^2} \right\} P(\tau) \quad (80)$$

$$\eta_M = \frac{\cos(\Omega \tau - 2i \omega) - \cosh(\omega) \cosh(qz)}{\cosh(\Omega \tau) - \cos(\omega) \cos(qz)} P(\tau) \quad (81)$$

with $q' = 2 \sinh(\omega)$, $\Omega = 2 \sinh(2\omega)$ and Ω real and related to the time period $2\pi/\Omega$ and

$$P(\tau) = n(\tau) \exp \left[-i \frac{Dz^2}{n(\tau)} \right] \exp[2i \tau]$$

5. CONCLUSIONS

In the first part of the paper, we have derived a linear Miles’ theory for waves propagating on finite depth h . The well known Miles’ theory has been extended to the finite depth under breeze to moderate winds conditions. The equations of motion governing the dynamics of the air/water interface in finite depth have been linearized and we have studied the linear time instability of a normal Fourier mode k . The prediction of exponential growth of wave amplitude (or energy) is well confirmed by field and laboratory experiments (the wind-to-waves energy transfer rates predictions are smaller than the observations, although their order of magnitude is the same). In the second part we have derived, two wind-forced finite depth model equations: an anti-diffusive Korteweg-de Vries-Burger equation and an anti-diffusive nonlinear Schrödinger equation in finite depth. For KdV-B the blow-up time and the breaking time of wind soliton solutions have been established in terms of physical parameters. For the anti-diffusive nonlinear Schrödinger equation in finite depth we have exhibited the Akhmediev the Peregrine and the Ma solutions for weak wind inputs in finite depth. There are many other parameters such as variations of wind speed and direction, coastal geometry and bathymetry, bottom friction, surface drift, boundary layer turbulence, non-linear waves interactions, that influence the growth of wind-waves in finite depth. Taking into account these phenomena represents a work that cannot be handled analytically. Our study is highly idealized, however it may provide a valuable insight about the effect of depth on the mechanism of water wave amplification by wind and be useful in theoretical forecast of wind-wave growth rates in finite depth.

Annexe A : Summary table

Summary table of linear, quasi-linear and nonlinear approaches

Miles’ Theory	Linear model	Rayleigh equation
	Quasi-linear approach	NSL equation
Jeffrys’ Theory	Linear approximation	Exponential growth of wave amplitude
	Nonlinear model	KdV-Burger equation

Annexe B : Coefficients of equations (73) and (74)

The coefficients c_g, a, b and d of the perturbed NLS Eq. (72) are

$$c_g = \frac{c}{2} \left[1 + \frac{2kh}{\sinh(2kh)} \right],$$

$$a = -\frac{1}{2\omega} \left[c_g^2 - gh[1 - khT(1 - T^2)] \right],$$

$$b = \frac{k^4 c^2}{4\omega} \left\{ \frac{9}{T^4} - 12 + 13T^4 - 2T^6 - \frac{2 \left[2c + c_g(1 - T^2) \right]^2}{T^2 (gh - c_g^2)} \right\},$$

$$d = \frac{\varepsilon\beta(U_1)^2}{2c^2} T\omega$$

The coefficients $c_g, A, B,$ and D of the dimensionless wind-forced NLS Eq. (73) are

$$c_g = \frac{1}{2\theta_{fd}} \left[1 + \frac{\delta}{\theta_{dw}^2} \left(\frac{1 - T^2}{T} \right) \right],$$

$$A = -\frac{c_g^2}{2\theta_{fd}\theta_{dw}^2} - \frac{\delta}{2\theta_{fd}} \left[\theta_{fw}^2 - \delta(1 - T^2) \right],$$

$$B = \frac{1}{4\theta_{fd}^3\theta_{dw}^2} \{ 9 - 12T^2 + 13T^4 - 2T^6 - \frac{2 \left[2\theta_{fd}^{-1} + c_g(1 - T^2) \right]^2}{(\delta - c_g^2)T^2} \},$$

$$D = \frac{\varepsilon\beta\sqrt{T}}{2\theta_{dw}^3}.$$

ACKNOWLEDGMENTS

This work has been supported by the Center for International Scientific Studies & Collaboration (CISSC).

REFERENCES

Akhmediev, N. N., V. M. Eleonskii and N. E. Kulagin (1987). Exact first-order solutions of the nonlinear Schrödinger equation. *Theor. Math. Phys.* 72, 809.

Beji, S. and K. Nadaoka (2004). Solution of Rayleigh’s instability equation for arbitrary wind profiles. *J. Fluid Mech.* 500, 65-73.

Belcher, S. E. and J. C. R. Hunt (1993). Turbulent shear flow over slowly moving waves. *Journal of Fluid Mechanics* 251, 109-148.

Benney, D. J. (1996). Long waves on liquid films. *Journal of Mathematical Physics* 45, 150–155.

Bretschneider, C. L. (1958). *Revised wave forecasting relationships*. Proceedings of the 6th conference on Coastal Engineering, Gainesville/Palm Beach/Miami Beach, F.L.

- ASCE, New York 30-67.
- Charnock, H. (1995). Wind stress on a water surface. *Quart. J. Roy. Meteorol. Soc.* 81, 639.
- Donelan, M. A., A. V. Babanin, I. R. Young and M. L. Banner (2006). Wave-follower field measurements of the wind-input spectral function. Part II: Parameterization of the wind input. *Journal of Physical Oceanography* 36, 1672-1689.
- Dysthe K. B. and K. Trulsen (1999). Note on Breather Type Solutions of the NLS as Models for Freak-Waves. *Physica Scripta* T82, 48.
- Fairall, C. W., A. A. Grachev, A. Bedard and R. T. Nishiyama (1996). *Wind, Wave, Stress and Surface Roughness Relationships from Turbulence Measurements made on R/P flip in the Scope Experiment*. NOAA technical memorandum ERL ETL-268.
- Fenton, J. D. (1979). A high-order cnoidal wave theory. *J. Fluid Mech.* 94, 129-161.
- Francius M. and C. Kharif (2006). Three-dimensional instabilities of periodic gravity waves in shallow water. *J. Fluid Mech.* 561, 417.
- Garratt, J. R., G. D. Hess, W. L. Physick and P. Bougeault (1996). The Atmospheric Boundary Layer-Advances in Knowledge and Application. *Boundary Layer Meteorology* 78, 9-37.
- Grad, H. and P. W. Hu (1967). Unified shock profile in a plasma. *Physics of Fluids* 10, 2596-2602.
- Hu, P. (1972). Collisional theory of shock and nonlinear waves in a Plasma. *Physics of Fluids* 15, 854-864.
- Ijima, T. and F. L. W. Tang (2011). *Numerical calculation of wind waves in shallow water*. Coastal Engineering Proceedings, North America.
- Janssen, P. A. E. M. (1991) Quasi-linear theory of wind generation applied to wave forecasting. *J Phys Oceanogr* 21, 1631.
- Janssen, P. A. E. M. (2004). *The Interaction of Ocean Waves and Wind*. Cambridge University Press.
- Jeffrey, A. and S. Xu (1989). Exact solutions to the Korteweg-de Vries-Burgers equation. *Wave Motion* 11, 559.
- Jeffreys, H. (1924). On the formation of waves by wind. *Proceedings of the Royal Society of London. Series A: Mathematical and Physical Sciences* A107, 189-206.
- Jeffreys, H. (1925). On the formation of waves by wind II. *Proceedings of the Royal Society of London. Series A: Mathematical and Physical Sciences* A110, 341-347.
- Johnson, R. S. (1972). Shallow water waves on a viscous fluid-the nodular bore. *Physics of Fluids* 15, 1693-1699.
- Karahara, T. (1970). Weak nonlinear magneto-acoustic waves in a cold plasma in the presence of effective electron-ion collisions. *J. Phys. Soc. Japan* 27 1321-9.
- Kharif, C., J. P. Giovanangeli, J. Toublon, L. Grade and E. Pelinovski (2008). Influence of wind on extreme wave events: experimental and numerical approaches. *Journal of Fluid Mechanics* 594, 209-247.
- Kharif, C., R. Kraenkel, M. A. Manna and R. Thomas (2010). The modulational instability in deep water under the action of wind and dissipation. *J. Fluid Mech.* 664, 138.
- Korteweg, D. J. and G. de Vries (1895). On the change of form of long waves advancing in a rectangular canal, and a new type of stationary waves. *Philosophical Magazine* 39, 422-443.
- Lighthill, M. (1925). *Waves in Fluids*. Edited by C. U. Press.
- Ma, Y. (1979). The Perturbed Plane-Wave Solutions of the Cubic Schrödinger Equation. *Stud. Appl. Math* 60, 43.
- Makin, V. (2004). A Note on the Drag of the Sea Surface at Hurricane Winds. *Boundary-layer meteorology* 115, 169-176.
- Manna, M. A., P. Montalvo and R. A Kraenkel (2014). Finite time blow-up and breaking of solitary wind waves. *Physical Review E* 90, 013006
- McCowan, J. (1894). On the Highest Wave of Permanent Type. *Philosophical Magazine Series* 5(38), 351.
- Miche, R. (1944). *Mouvements ondulatoires de la mer en profondeur constante ou décroissante*. Edited by A. des Ponts et Chausses.
- Miles, J. W. (1957). On the generation of surface waves by i-ows. *Journal of Fluid Mechanics* 3, 185-204.
- Miles, J. W. (1997). Generation of surface waves by winds. *Applied Mechanics Reviews* 50-7, R5-R9.
- Montalvo, P., J. Dorignac, M. A. Manna, C. Kharif and H. Branger (2013a). Growth of surface wind-wave in water of finite depth. *A theoretical approach. Coastal Engineering* 77,

- 49-56.
- Montalvo, P., R. Kraenkel, M. A. Manna and C. Kharif (2013b). Wind-wave amplification mechanisms: possible models for steep wave events in finite depth. *Natural Hazards and Earth System Sciences* 13, 2805-2813
- Onorato, M. and D. Proment (2012). Approximate rogue wave solutions of the forced and damped Nonlinear Schrödinger Equation for water waves. *Physics Letters A* 376, 3057-3059.
- Ott, E. and R. Sudan (1970). Damping of Solitary Waves. *Phys. Fluids* 13, 1432.
- Peregrine, D. and J. Austral (1983). Water waves, nonlinear Schrödinger equations and their solutions. *Math. Soc. Ser. B* 25(1), 16.
- Phillips, O. M. (1957). On the generation of waves by turbulent wind. *Journal of Fluid Mechanics* 2, 417-445.
- Pierson, W. J. and L. Mokowitz (1964). A proposed spectral form for fully developed wind seas based on the similarity theory of S.A. Kitaigorotskii. *Journal of Geophysical Research* 69, 5181-5189.
- Rayleigh, L. (1880). On the stability or instability of certain fluid motions. *Proceedings of the London Mathematics Society* XI, 57-70.
- Shemer, L. (2013). On kinematics of very steep waves. *Nat. Hazards Earth Syst. Sci.* 13, 2101.
- Tennekes, H. (1972). The logarithmic wind profile. *Journal of the atmospheric sciences* 30, 234.
- Thijsse, T. J. (1949). *Dimensions of wind-generated waves*. General assembly of Association d'Océanographie physique. Procés-Verbaux 4, 80-81.
- Thomas, C. Kharif, and M. A. Manna (2012). A nonlinear Schrödinger equation for water waves on finite depth with constant vorticity. *Phys. Fluids* 138.
- Toublon, J. and C. Kharif (2006). On the interaction of wind and extreme gravity waves due to modulational instability. *Physics of Fluids* 18, 108103-1 – 108103-4.
- Touboul, J., C. Kharif, E. Pelinovsky and J. P. Giovanangeli (2008). On the interaction of wind and steep gravity wave groups using Miles' and Jeffreys' mechanisms. *Nonlin. Processes Geophys.* 15, 1023.
- Wadati, M. (1975). Wave Propagation in Nonlinear Lattice. *Journal of the Physical Society of Japan* 38, 673-680.
- Whitham, G. (1974). *Linear and Nonlinear Waves*. Wiley Interscience, New York.
- Wu, J. (1982). Wind-stress coefficients over sea surface from breeze to hurricane. *Journal of geophysical research* 87, Issue C12, 9704–9706.
- Young, I. R. and L. A. Verhagen (1966a). The growth of fetch limited waves in water of finite depth. Part I: total energy and peak frequency. *Coastal Engineering* 29, 47-78.
- Young, I. R. and L. A. Verhagen (1966b). The growth of fetch limited waves in water of finite depth. Part II: spectral evolution. *Coastal Engineering* 29, 79-99.
- Young, I. R. (1997a). The growth rate of finite depth wind-generated waves. *Coastal Engineering* 32, 181-195.
- Young, I. R. (1997b). *Wind Generated Ocean Waves*. Elsevier.
- Young, I. R. and A. Babanin (2006). Spectral distribution of energy dissipation of wind-generated waves due to dominant wave braking. *Journal of physical Oceanography* 36, 376-394.